# Stabilizing interaction of exopolymers with nano-Se and impact on mercury immobilization in soil and groundwater

Wang, Xiaonan; Song, Wenjuan; Qian, Haifeng; Zhang, Daoyong; Pan, Xiangliang; Gadd, Geoffrey Michael

*Published in:*
Environmental Science: Nano

*DOI:*
10.1039/c7en00628d

*Publication date:*
2018

Lin kto Final version published in Environmental Science: 10.1039/c7en00628d

# Stabilizing Interaction of Exopolymers with Nano-Se and Impact on Mercury Immobilization in Soil and Groundwater

Xiaonan Wang [a, c], Wenjuan Song[a], Haifeng Qian [a, b], Daoyong Zhang[a, b], Xiangliang Pan [a, b, *] Geoffrey Michael Gadd [d]

[a] *Xinjiang Key Laboratory of Environmental Pollution and Bioremediation, Xinjiang Institute of Ecology and Geography, Chinese Academy of Sciences, Urumqi 830011, China*

[b] *College of Environment, Zhejiang University of Technology, Hangzhou 310014, China*

[c] *University of Chinese Academy of Sciences, Beijing 100049, China*

[d] *Geomicrobiology Group, School of Life Sciences, University of Dundee, Dundee DD15EH, Scotland, UK*

*For correspondence. E-mail panxl@zjut.edu.cn; Tel. +86 571 88320634; Fax +86 571 88320634.

**Running title**: EPS enhance mercury remediation by SeNPs

## ABSTRACT

Remediation of metal-contaminated soils and waters using nanoparticles is highly limited by their strong tendency to aggregate in soil solution and natural water. In order to enhance remediation of $Hg^0$ contaminated soil solution and groundwater by SeNPs (Se nanoparticles), the effects of extracellular polymeric substances (EPS) on the stability of SeNPs and $Hg^0$ removal were investigated. EPS from the selenite-reducing bacterium *Citrobacter freundii* Y9 was found to make SeNPs more negatively charged by strong adsorption which significantly enhanced the stability of SeNPs. The protein, carboxylate, polysaccharide and lipid components of the EPS were involved in the adsorption to SeNPs. Fluorescence quenching titration measurementss implied that the binding of proteinaceous substances in the EPS to SeNPs was static quenching. EPS can therefore enhance the remediation efficiency of SeNPs for soil solution and groundwater contaminated with $Hg^0$. This study highlights that bacterial EPS can be used as an effective natural dispersant for SeNPs therefore improving the efficiency of mercury immobilization is contaminated waters.



**Keywords:** Aggregation; dispersant; EPS; fluorescence quenching titration; remediation; mercury; selenium

## Introduction

Nanoparticles have received considerable attention for their potential application in the remediation of metal-contaminated sites because of their high chemical and biological reactivity.[1] However, remediation of contaminated soils and waters using nanomaterials is highly challenging because there is a strong tendency for agglomeration of nanoparticles in the soil or sediment solutions which results in limited dispersion and thus substantially reduces the remediation performance. Moreover, nanoparticles readily anchor onto various solid matrices in soil. It is therefore of great importance to maintain the dispersion properties of nanoparticles.

Two approaches have been proposed to improve dispersion of nanoparticles: steric and electrostatic stabilization.[2] Steric stability can be provided by dispersants which tightly bind to the nanoparticle surface and surface charge can be imparted or increased to enhance electrostatic repulsion. Some studies have shown that dispersants can significantly improve nanoparticle stability and mobility in both water and soil.[3,4] However, the wide use of chemically produced polymeric dispersants provides another challenge to the environment. Therefore, it is desirable to seek natural and environmentally-friendly dispersants to stabilize nanoparticles.

Some natural organic matter (NOM), such as humic substances, can increase electrostatic repulsion or steric stability of nanoparticles by binding to the nanoparticles which subsequently modifies their surface chemistry and charge.[5]

However, effects of NOM on the stability of nanoparticles reported in the literature are contradictory. Some studies showed that organic matter contributes to the formation of densely aggregated nanoparticulate ZnS.[6] Some proteins strongly bound to nanoparticles can decrease their size which is similar to the effects of surfactants.[7] Similarly, microbial extracellular polymeric substances (EPS), which are composed of a variety of organic substances such as carbohydrates, proteins, uronic acids and deoxyribonucleic acids, may either limit the dispersal or, in contrast, stabilize the nanoparticles.[8-10]

Selenium nanoparticles (SeNPs) have been extensively used in a variety of industries such as electronics and photonics. Biological methods have been explored to synthesis SeNPs by reduction of selenium oxyanions, which is also considered to be an effective bioremediation technique for selenium removal.[11-13] Recently, SeNPs have been used for remediation of elemental mercury ($Hg^0$) contamination based on the reaction: $Hg^0 + Se^0 \rightarrow HgSe$, because $Se^0$ is prone to reacting with $Hg^0$ to form HgSe ($\Delta G^0$ of -38.1 kJ $mol^{-1}$), the most stable inorganic mercury compound with a *Ksp* of $1.0\times10^{-59}$.[14-16] Normally, elemental mercury comprises only a small proportion of the total mercury in soil whereas in mercury or gold mining regions and in chlor-alkali plant soil, elemental mercury account for a huge part of the total mercury[17-19]. Furthermore, dissolved elemental mercury is a significant mercury species in natural waters, for instance, dissolved elemental mercury production

(~0.4-3.5% $d^{-1}$ of dissolved total mercury) was an important influence on the fate of mercury in Long Island Sound.[20] The remediation efficiency of SeNPs for mercury contaminated soil and water could be highly limited by their aggregation in the complex soil solution or natural waters.

EPS is responsible for the colloidal properties of SeNPs, which govern the fate of SeNPs in the environment and bioremediation performance.[21,22] Therefore, it is essential to investigate the effects of EPS on SeNPs under natural conditions and the impact on mercury remediation using SeNPs.

In this study, the binding ability of EPS to SeNPs and resulting modification of the SeNPs surface were examined by fluorescence excitation emission matrix (EEM) spectroscopy, fluorescence quenching titration, Fourier transform infrared spectroscopy (FTIR) and potentiometric titrations. Hydrodynamic diameter distribution, zeta potential, and settling efficiency of SeNPs in the absence and presence of EPS were measured to investigate effects of EPS on the stability of SeNPs. Finally, the impacts of EPS on elemental mercury immobilization by SeNPs were also investigated.

## Experimental

### Extraction and characterization of EPS

The SeNP producing bacterium *Citrobacter freundii* Y9, isolated from

anaerobic sulfate-reducing sludge, was cultivated at 30°C in a medium containing 1.0 g $K_2HPO_4$, 0.1 g $MgCl_2$, 0.2% yeast extract, 10 mM { HYPERLINK "http://dict.cn/sodium%20citrate" } in 1 L Milli-Q water (18 $M\Omega cm^{-1}$). To extract EPS, *C. freundii* Y9 culture was firstly centrifuged (Anke GL-20G-Ⅱ, Shanghai, China)at 3300 g × 10 min at 4°C. The harvested biomass was re-suspended in Milli-Q water and centrifuged again at 16600 g for 20 min at 4°C. The supernatant was filtered using 0.45 μm pore size membranes and then purified using a dialysis membrane (3500 Da) at 4°C for 24 h.[23] Total organic carbon (TOC) content of EPS solution was quantified by a TOC analyzer (TOC-4100, Shimadzu, Japan). The content of polysaccharides and proteins was measured by the phenol-sulfuric acid method and the Lowry method, respectively.[24,25]

**Soil solution and ground water**

The effects of EPS on SeNPs was investigated in groundwater and soil solution. Groundwater, taken from Urumqi, Xinjiang, China, was filtered through 0.45 μm membranes and then kept at 4°C. Soil solution was prepared according to the following protocol. 10 g of soil taken from farmland was mixed with 50 ml Milli-Q water and shaken for 18 h. The mixture was centrifuged for 20 min at 4400 g and the supernatant filtered through 0.45 μm membranes.[26] After that the soil solution was purified with a dialysis membrane (500 Da) at 4°C for 24 h in order to remove dissolved organic matter. TOC of ground water and soil solution was measured as

described above. pH was measured using a Mettler Seven Easy pH meter (Mettler Toledo, Greifensee, Switzerland), conductivity was determined with a DDSJ-308A conductivity meter (REX Instrument Factory, Shanghai, China), $Cl^-$ and $SO_4^{2-}$ were analyzed using a Dionex ICS 5000 ion chromatograph (Thermo Fisher Scientific, Waltham, USA), $CO_3^{2-}$ and $HCO_3^-$ were analysed using a Mettler-Toledo G20 automatic titrator (Mettler Toledo, Greifensee, Switzerland), $K^+$, $Ca^{2+}$, $Na^+$, $Mg^{2+}$ were quantified by ICP-OES 735-ES (Agilent Technologies, Tokyo, Japan). The physico-chemical properties of the soil solution included pH (7.99), conductivity (456 μS $cm^{-1}$), TOC (11.38 mg $L^{-1}$), $Cl^-$ (24.57 mg $L^{-1}$), $SO_4^{2-}$ (95.79 mg $L^{-1}$), $Ca^{2+}$ (73.96 mg $L^{-1}$), $K^+$ (1.51 mg $L^{-1}$), $Mg^{2+}$ (9.85 mg $L^{-1}$), $Na^+$ (34.56 mg $L^{-1}$), $CO_3^{2-}$ (0 mg $L^{-1}$) and $HCO_3^-$ (160.63 mg $L^{-1}$). The physico-chemical composition of groundwater included pH (8.42), conductivity (1153 μS $cm^{-1}$), TOC (1.17 mg $L^{-1}$), $Cl^-$ (76.95 mg $L^{-1}$), $SO_4^{2-}$ (352.49 mg $L^{-1}$), $Ca^{2+}$ (6.74 mg $L^{-1}$), $K^+$ (20.22 mg $L^{-1}$), $Mg^{2+}$ (8.41 mg $L^{-1}$), $Na^+$ (254.80 mg $L^{-1}$), $CO_3^{2-}$ (0 mg $L^{-1}$) and $HCO_3^-$ (175.48 mg $L^{-1}$).

**Preparation of SeNPs and EPS-capped CheSeNPs**

Chemically synthesized SeNPs (CheSeNPs) were synthesized by reduction of sodium selenite with ascorbic acid. The produced SeNPs were purified according to the following protocol.[27] The SeNPs supernatant was sonicated in a digital ultrasonic bath (Hu20500B, Tianjin, China) followed by hexane separation and then

collected by centrifugation at 10000 g and 4°C for 10 min. After that CheSeNPs were freeze-dried in a vacuum freeze dryer (Labconco, Kansas, USA). f

Biological SeNPs (BioSeNPs) were obtained by bioreduction of 1 mM selenite by *C. freundii* Y9. Supernatants were collected by centrifugation at 10000 g and 4°C for 10 min, and then purified as follows.[28] The precipitate was washed with Tris-HCl (10 mM, pH 7.4) two times and re-suspended in 2% (w/v) sodium dodecyl sulfate and 0.2 M NaOH. After that the precipitate was put in ultrasonic cell disruptor (Scientz Biotechnology, Ningbo, China) at 120 W for 10 min in an ice bath, then centrifuged (10000 g, 4°C, 10 min) and washed with Milli-Q water more than three times. Finally, the precipitate was freeze-dried.

To obtain SeNPs capped by 20 and 100 mg $L^{-1}$ EPS, CheSeNPs were added into 20 or 100 mg $L^{-1}$ EPS containing soil solution or groundwater and mixed at 200 rpm using a magnetic stirrer for 6 h (Jinyi Technology, Jintan, China) and sonicated (Hengao Technology, Tianjin, China) for 5 min. Afterwards, the precipitate was harvested by centrifugation at 10000 g and 4°C for 10 min and freeze-dried. The concentration of CheSeNPs used was 100 mg $L^{-1}$ unless otherwise stated.

**Characterization of CheSeNPs and EPS-capped CheSeNPs**

Hydrodynamic diameter distribution and zeta potential of CheSeNPs and EPS-capped CheSeNPs were measured using a laser size distribution analyzer (Zetasizer Nano ZS90, Malvern, Worcestershire, UK). For hydrodynamic diameter

157 distribution measurements, samples were prepared as follows. 1 mg sample was
158 added to 10 ml soil solution or groundwater and sonicated (Hengao Technology,
159 Tianjin, China) for 15 min and the hydrodynamic diameter distribution was
160 measured immediately. The zeta potential of SeNPs in the soil solution or
161 groundwater at different pH values was measured as follows. Soil solution or
162 groundwater pH was carefully adjusted using NaOH (0.1 M) and HCl (0.1 M) to pH
163 of 3, 5, 7, 9 or 11. Then 1 mg sample was added to 10 ml soil solution/groundwater
164 and the mixture sonicated for 30 min. EPS was used as a control for zeta potential
165 measurements. Zeta potential was calculated based on the Smoluchowski
166 approximation, and for each measurement, samples were first equilibrated for 120 s
167 and zeta-potential detection carried out in triplicate.

168 To determine $pK_a$ and the surface charge of CheSeNPs and EPS-capped
169 CheSeNPs, potentiometric titration was carried out using a Metrohm 702 SM
170 potentiometric titrator (Metrohm Ltd., Herisau, Switzerland). 0.01 g sample was
171 dissolved in 50 ml background electrolyte (0.1 M $NaNO_3$). The initial pH of solution
172 was decreased to ~2 using 0.1 M HCl. The titration was conducted by automatic
173 addition of 0.02 ml aliquots of NaOH (0.1 M). For the control titration, 200 mg $L^{-1}$
174 EPS containing $NaNO_3$ (0.1 M) was performed separately.

175 **FTIR spectroscopical analysis**

176 For FTIR analysis, about 1 mg sample was ground with 100 mg KBr in an

agate mortar. FTIR spectra over the range 4000-400 $cm^{-1}$ at a resolution of 4 $cm^{-1}$ were detected by a Bruker Vertex 70/V spectrometer (Bruker, Berlin, Germany) equipped with a D-LaTGS-detector. All samples were scanned three times to determine the changes in vibration frequency of the functional groups, with no significant difference between the spectra. The background obtained from the scanning of pure KBr was automatically subtracted from the sample spectra.

**Fluorescence spectroscopy and quenching titration**

3D excitation and emission fluorescence spectroscopy of EPS was obtained using a Hitachi F-7000 fluorescence spectrophotometer (Hitachi, Tokyo, Japan) equipped with a 1.0 cm quartz cell and a thermostatic bath. The EEM spectra were collected at 5 nm increments over an excitation range of 200-500 nm, with an emission range of 200-500 nm every 2 nm with an excitation/emission slit of 5.0 nm. The scanning speed was 1200 nm $min^{-1}$. Milli-Q water was set as the blank which was subtracted from the sample EEM spectra. EEM spectral images were generated using SigmaPlot 10.0 (Systat, US). EPS solutions were titrated with incremental μL addition of 4.22 mM CheSeNPs suspension at 298 K. After each addition of SeNPs solution, the solution was fully mixed using a magnetic stirrer for 15 min and the fluorescence spectra recorded. The equilibrium time was set as 15 min since fluorescence intensities at peaks varied little after 15 min reaction time.

**Settling experiments**

The settling experiments for 100 mg $L^{-1}$ of CheSeNPs/EPS-capped CheSeNPs were conducted in soil solution, groundwater and Milli-Q water. The suspensions were homogenized in an ultrasonic bath (Hu20500B, Tianjin, China) at 35 kHz and 240 W for 20 min. $OD_{600nm}$ was measured 3 cm below the liquid surface using a Cary 60 UV-Vis spectrophotometer (Agilent Technology, Santa Clara, USA), which represents the concentration of SeNPs.

**Impact of EPS on mercury remediation using SeNPs**

The impact of EPS on mercury immobilization using SeNPs was conducted in $Hg^0$ contaminated groundwater (Fig. S1). $Hg^0$ contaminated ground water was prepared according to a previous study as follows.[29] A small droplet of elemental Hg was added into ground water which had already been purged for 30 min in a sonicator (Hengao Technology, Tianjin, China). After that, the solution was sonicated for another 30 min and then stabilized overnight:the supernatant was collected as $Hg^0$ contaminated groundwater. The $Hg^0$ solution was used within 2 h to avoid oxidation. 100 ml $Hg^0$ contaminated groundwater/soil solution containing 50 mg $L^{-1}$ SeNPs in the presence of 0, 1, 10, 50, 100, 200 mg $L^{-1}$ of EPS were added into a 500 ml jar. CheSeNPs and BioSeNPs were both used in the present study. The sealed jar was shaken at 130 rpm in an incubator shaker (Crystal IS-RSV3, Dallas, USA) overnight, and after that the $Hg^0$ concentration was measured using a mercury analyzer (Lumex RA915+, Saint Petersburg, Russia). For mercury analysis, the high

concentration mode was selected and an additional cell for analysis was used.The sample flow rate was set 1.0 L $min^{-1}$, and $KMnO_4$ solution (5%) was used to capture mercury-containing waste gas. A control without the supply of SeNPs and EPS was also conducted.

All the experiments were conducted in triplicate and mean values were used.

## Results

### Fluorescence quenching titration of EPS with CheSeNPs

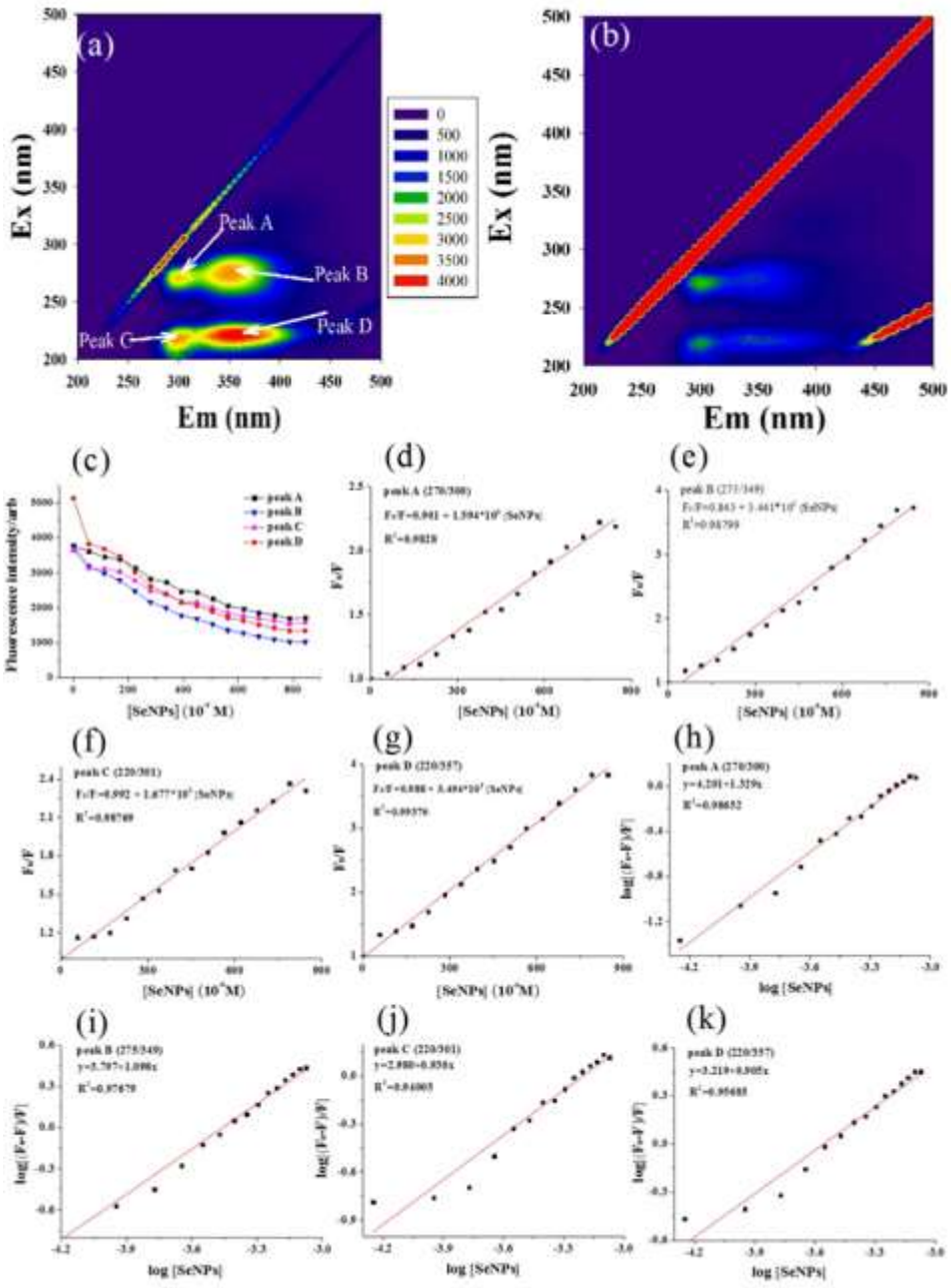


225

226 Fig. 1. (a) Typical three-dimensional fluorescence EEM spectrum of EPS; (b) three-
227 dimensional fluorescence EEM spectrum of EPS after addition of 4.22 mM
228 CheSeNPs; (c) fluorescence quenching curves of EPS titrated with CheSeNPs
229 solution. Values represent means ± standard deviation of three independent

measurements. Bars indicate standard errors. (d) (e) (f) (g) are the Stern-Volmer plots of fluorescence quenching of the peaks A, B, C and D of EPS titrated with CheSeNPs solution. (h) (i) (j) (k) are the plots of log [($F_0$-F)/F] versus log [SeNPs] of fluorescence quenching of the peaks A, B, C and D of EPS titrated with CheSeNPs suspension.

The EPS solution had a TOC content of 163.0 mg $L^{-1}$, with 19.1 mg $L^{-1}$ polysaccharide and 87.3 mg $L^{-1}$ protein. The EEM fluorescence spectrum of EPS showed the presence of four distinct peaks (Fig. 1a). The four peaks were designated peaks A (Ex/Em=270/300), B (Ex/Em=275/349), C (Ex/Em=220/301) and D (Ex/Em=220/357). The fluorescence intensity of these peaks significantly decreased with the incremental addition of CheSeNPs (Fig. 1b, c), indicating strong binding of EPS to the CheSeNPs. In order to obtain the binding parameters, the fluorescence quenching data were further fitted to the Stern-Volmer equation (1) and the Hill equation (2).[30,31]

$$F_0/F = 1 + k_q\tau_0 [\text{CheSeNPs}] = 1 + K_{SV}[\text{CheSeNPs}] \quad (1)$$

where $F_0$ and $F$ are the fluorescence intensities in the absence or presence of quencher; $K_q$ = quenching rate constant; $K_{sv}$ = quenching constant; $\tau_0$ = average lifetime of the fluorescence in the absence of quencher which is usually taken as $10^{-8}$ s and [CheSeNPs] = concentration of CheSeNPs. The fluorescence quenching

data well fitted to the Stern-Volmer equation (Fig. 6d, e, f, g). $K_{sv}$ ($\times 10^3$ L mol$^{-1}$) estimated from the Stern-Volmer equation for peaks A, B, C and D were was 1.59 ($R^2$=0.98), 3.44 ($R^2$=0.99), 1.68 ($R^2$=0.99) and 3.49 ($R^2$=0.99), respectively. The calculated $K_q$ ($\times 10^{11}$ L mol$^{-1}$ sec$^{-1}$) was as follows: 1.59, 3.44, 1.68, and 3.49.

Fluorescence intensity data were also used to estimate the binding constant ($K_b$) and the number of binding sites ($n$) for binding of EPS to CheSeNPs using the Hill equation (2):

$$\log [(F_0\text{-}F)/F] = \log K_b + n\log[\text{CheSeNPs}] \quad (2)$$

where ($F_0$-$F$) = fraction of quenched fluorescence with CheSeNPs binding; $K_b$ = a binding constant that reflects the interactive intensity between the fluorophore and a quencher; $n$ = equivalent binding sites provided by fluorophore to the quencher molecule. A good linear relationship was obtained between log［($F_0$-$F$)/$F$］and log ［CheSeNPs］(Fig. 6h, i, j, k). The binding constant ($K_b$, $\times 10^3$ L mol$^{-1}$) for peaks A, B, C and D were 15.9, 6.3, 0.95 and 1.7 respectively and $n$ for peaks A, B, C and D were 1.33, 1.10, 0.93 and 0.91, respectively.

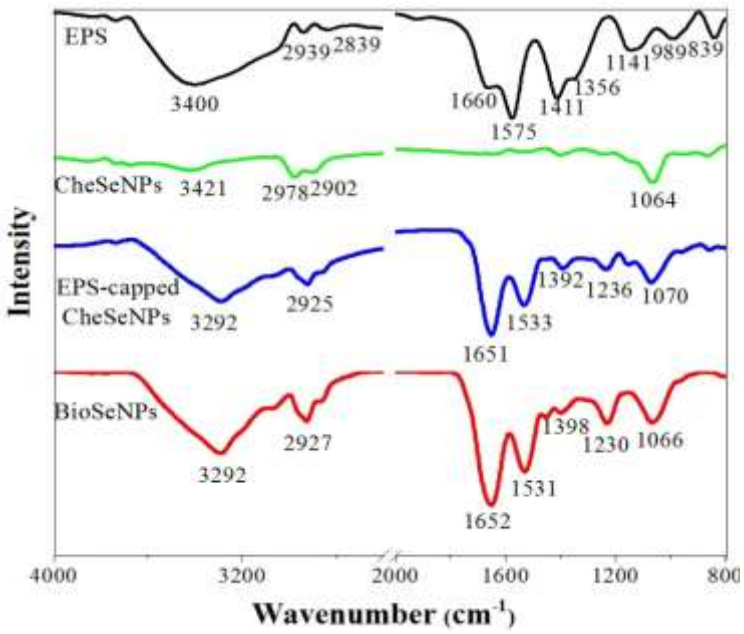


Fig. 2. FTIR spectra of EPS, BioSeNPs, CheSeNPs and EPS-capped CheSeNPs. Typical results are shown from one of several determinations.

**FTIR spectroscopical analysis**

The FTIR spectrum of the EPS (Fig. 2) showed a broad –OH stretch peak at 3400 $cm^{-1}$ and lipid –CH– vibration peaks at 2939 $cm^{-1}$ and 2839 $cm^{-1}$.[32,33] The peak at 1660 $cm^{-1}$ confirms the presence of the carbonyl stretch of the amide I group and the peak at 1575 $cm^{-1}$ shows the combination of N-H bending and C-N stretching of amide II functionalities.[34,35] The peak band appearing at 1411 $cm^{-1}$ is attributed to the symmetric stretching of the carboxylic group.[36] The 1356 $cm^{-1}$ peak indicates the adsorption band of C–H vibrations in the methyl group.[37] The peak at 1141 $cm^{-1}$ corresponds to polysaccharide groups and the peak at 839 $cm^{-1}$ can be designated as glycosidic linkage bonds.[35,38] The other minor absorption peaks ranging between

695-515 $cm^{-1}$ are due to the stretching of alkyl-halides, and the other bands in the fingerprint zone (<1000 $cm^{-1}$) might be attributed to phosphate groups.[39,40] After adsorption of EPS, peaks at 1651, 1533, 1392 and 1236 $cm^{-1}$ were observed in the FTIR spectrum of the EPS-capped CheSeNPs, indicating that the proteins, polysaccharides and lipids in the EPS were adsorbed to the CheSeNPs surface. The FTIR pattern of the EPS-capped CheSeNPs was similar to that of the BioSeNPs.

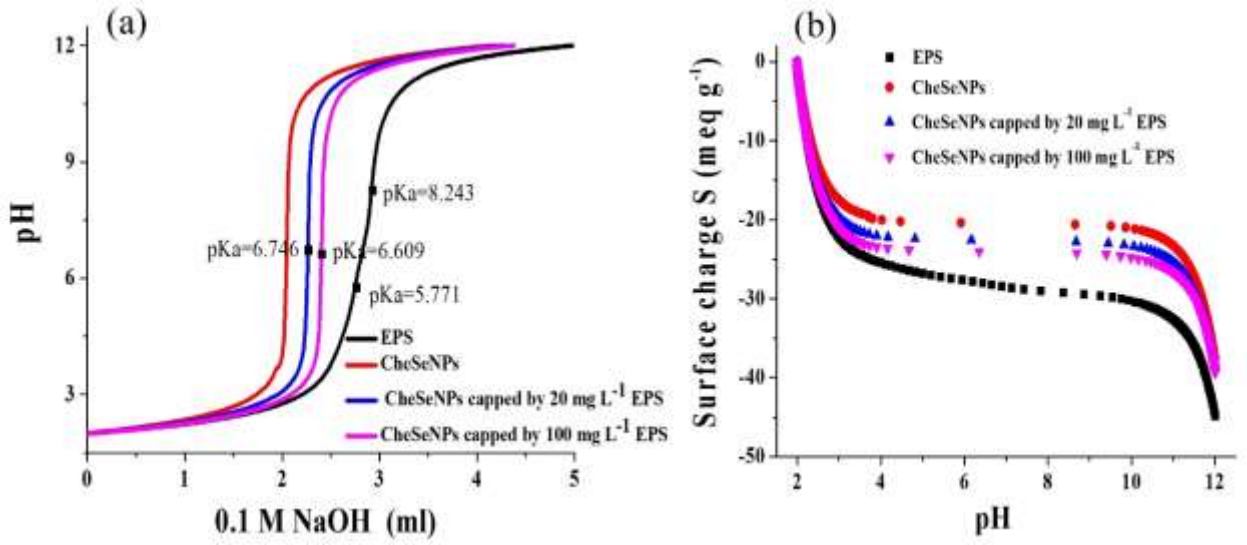


Fig. 3. (a) Acid-base titration curves of CheSeNPs, EPS-capped CheSeNPs and EPS, and (b) potentiometric titration curves of CheSeNPs, EPS-capped CheSeNPs and EPS. Surface charge was calculated according to the data from acid-base titrations. Typical patterns are shown from one of two determinations both of which gave similar results.

**Potentiometric titrations and Surface charge**

The acid-base titration curves for EPS showed a smooth increase of pH with

increasing amounts of NaOH (Fig. 3a). The buffering capacity followed an order of EPS >100 mg $L^{-1}$ EPS capped CheSeNPs > 20 mg $L^{-1}$ EPS capped CheSeNPs > CheSeNPs. The acid-base titration data of EPS showed the presence of two major functional groups with p$K_a$ values of 5.7 and 8.2. However, the p$K_a$ was 6.75 for 20 mg $L^{-1}$ EPS treated CheSeNPs and 6.61 for 100 mg $L^{-1}$ EPS treated CheSeNPs. It is seen from Fig. 3b that the surface charge became more negative with the increase of pH. The negative charge increased significantly between pH 2 and 4 because of the consumption of $H^+$ ions, and then leveled off until the pH increased up to 10 with the surplus supply of $OH^-$. The magnitude of surface charge number increased in the order of CheSeNPs < CheSeNPs capped by 20 mg $L^{-1}$ EPS < CheSeNPs capped by 100 mg $L^{-1}$ EPS< EPS.

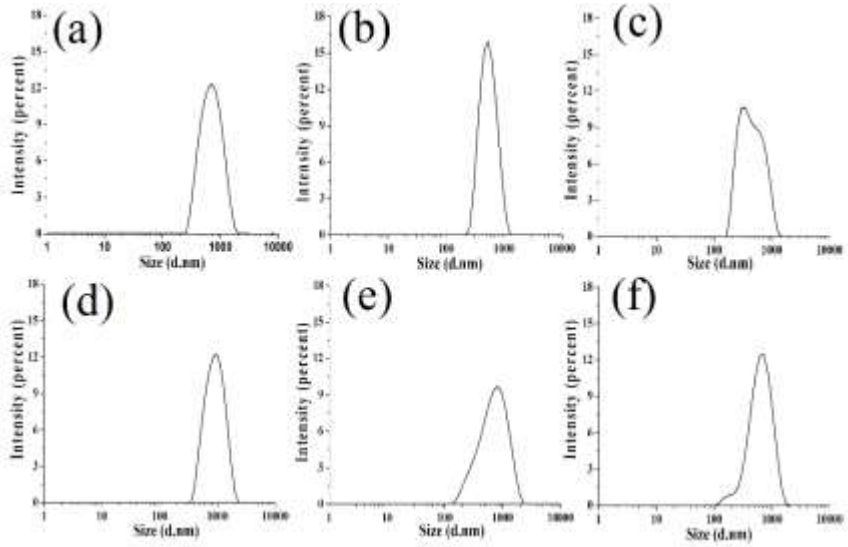


Fig. 4. Typical hydrodynamic diameter distribution curves of CheSeNPs (a), CheSeNPs capped by 20 mg $L^{-1}$ EPS (b) and CheSeNPs capped by 100 mg $L^{-1}$ EPS

306 (c) in ground water. Typical hydrodynamic diameter distribution curves of
307 CheSeNPs (d), CheSeNPs capped by 20 mg $L^{-1}$ EPS (e) and CheSeNPs capped by
308 100 mg $L^{-1}$ EPS (f) in soil solution. Typical curves are shown from one of several
309 determinations.
310
311 **Hydrodynamic diameter of SeNPs**
312 It is noted that the addition of EPS significantly changed the size distribution
313 pattern of CheSeNPs (Fig. 4). The average diameter of CheSeNPs in groundwater
314 was 740.2 nm, while in the presence of 20 and 100 mg $L^{-1}$ EPS, the average diameter
315 of CheSeNPs decreased to 556.9 and 484.3 nm, respectively. Similarly an average
316 diameter of CheSeNPs in soil solution was found to be 948.4 nm. However, the
317 addition of 20 and 100 mg $L^{-1}$ EPS solution decreased the average diameter of
318 CheSeNPs to 770.7 and 677.9 nm, respectively.
319 **Zeta potential of SeNPs**
320 The zeta potential as a function of pH for CheSeNPs, EPS-capped CheSeNPs
321 and EPS in soil solution/groundwater are shown in Fig. 5. It can be noted that the
322 zeta potential of EPS slightly changed over the pH range from pH 3 to 11 in both
323 groundwater and soil solution respectively. The average zeta value was -20.61 ± 1.29
324 and -28.02 ± 0.08 for EPS in groundwater and soil solution, respectively. These
325 values demonstrated that EPS suspension was colloidally stable. The zeta potential

of CheSeNPs significantly decreased when the pH increased from 3 to 11. However, in the presence of EPS, the zeta potential of EPS-capped CheSeNPs became more negative than CheSeNPs and this phenomenon was more predominant in groundwater compared to the soil solution. In groundwater, the magnitude of zeta potential was in the order CheSeNPs < CheSeNPs capped by 20 mg $L^{-1}$ EPS < EPS < CheSeNPs capped by 100 mg $L^{-1}$ EPS between pH 5 and 9. In the soil solution, the zeta potential of CheSeNPs capped by 100 mg $L^{-1}$ EPS was similar to EPS, which was higher than CheSeNPs capped by 20 mg $L^{-1}$ EPS and CheSeNPs.

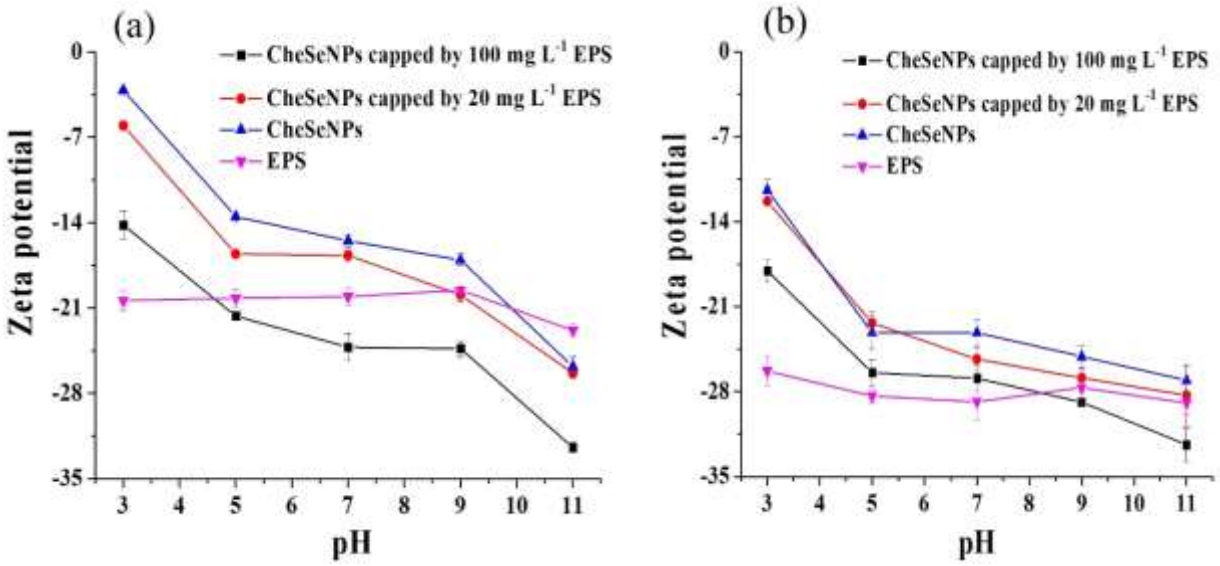


Fig. 5. (a) Zeta potential as a function of pH for CheSeNPs, EPS-capped CheSeNPs and EPS in the ground water; and (b) Zeta potential as a function of pH for CheSeNPs, EPS-capped CheSeNPs and EPS in the soil solution. Values represent the mean values of three independent measurements. Bars indicate standard errors.

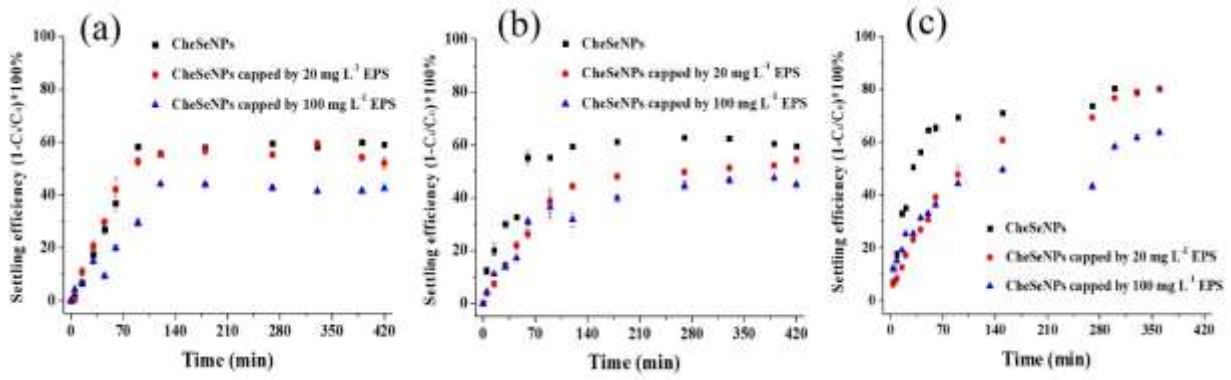


Fig. 6. Settling experiment of CheSeNPs and EPS-capped CheSeNPs in (a) groundwater, (b) soil solution, and (c) Milli-Q water. $C_i$ is the concentration of SeNPs detected over time, $C_0$ is the initial concentration of SeNPs. The concentration of SeNPs was indicated by $OD_{260nm}$ of the suspension. Error bars represent the standard deviation (n=3).

**Settling efficiency**

In groundwater, a slight difference of the settling efficiency between CheSeNPs capped by 20 mg $L^{-1}$ EPS (55.56%) and CheSeNPs (58.85%) was observed (Fig. 6a). However, this decreased to 42.78% for CheSeNPs capped by 100 mg $L^{-1}$ EPS. In soil extract, the settling efficiency significantly decreased with increasing concentration of EPS (Fig. 6b). It was noted that that 60.93% of CheSeNPs settled within 2 h in the absence of EPS while the presence of 20 and 100 mg $L^{-1}$ EPS slowed the settling process down to 51.83% and 45.89% respectively over 6 h. Similar settling experiments for CheSeNPs were performed in Milli-Q

356 water as controls. It is seen in Fig. 3c that CheSeNPs readily settled in 2 h with a
357 settling efficiency of 79.78% which was similar to the settling efficiency of
358 CheSeNPs capped by 20 mg $L^{-1}$ EPS over 6 h. However, the settling efficiency
359 decreased to 61.27% for CheSeNPs capped by 100 mg $L^{-1}$ EPS.

360 **Impact of EPS on mercury remediation using SeNPs**

361 The remediation efficiency of $Hg^0$ contaminated groundwater and soil
362 solution by BioSeNPs or CheSeNPs in the absence and presence of EPS are shown
363 in Fig. 7. In the case of groundwater, addition of 100 mg $L^{-1}$ BioSeNPs significantly
364 reduced the $Hg^0$ content from an initial 211 ng to 1.9 ng with a 99.1% removal
365 efficiency. The influence of EPS on $Hg^0$ remediation by BioSeNPs was not
366 significant. Addition of 1 mg $L^{-1}$ EPS slightly enhanced $Hg^0$ removal. However
367 higher concentrations of EPS showed little inhibition of $Hg^0$ removal efficiency. The
368 CheSeNPs showed a much lower removal efficiency, 73.5%, for $Hg^0$ in comparison
369 with the BioSeNPs. Addition of 1-200 mg $L^{-1}$ EPS generally increased $Hg^0$ removal.
370 Addition of 1 and 100 mg $L^{-1}$ EPS resulted in increases in the $Hg^0$ removal
371 percentage to 82.7% and 85.9%, respectively. The effect of EPS on $Hg^0$ removal in
372 the soil solution by BioSeNPs and CheSeNPs was similar to that in the groundwater.
373 However, much higher concentrations of EPS were required for improving $Hg^0$
374 removal from the soil solution than from the groundwater. 10 and 100 mg $L^{-1}$ EPS
375 were the optimal dosages for $Hg^0$ removal from the soil solution by BioSeNPs and

CheSeNPs, respectively. The possible reason for this may be the more complex composition of the soil solution than the groundwater.

It is found that most of the $Hg^0$ (over 88.8%) was removed as a precipitate from the groundwater and the soil solution by BioSeNPs and CheSeNPs in the absence and presence of EPS (Table 1). XRD analysis confirmed Hg in the precipitate was predominantly HgSe, which is the product of interaction between $Se^0$ and $Hg^0$ (Fig. 8).

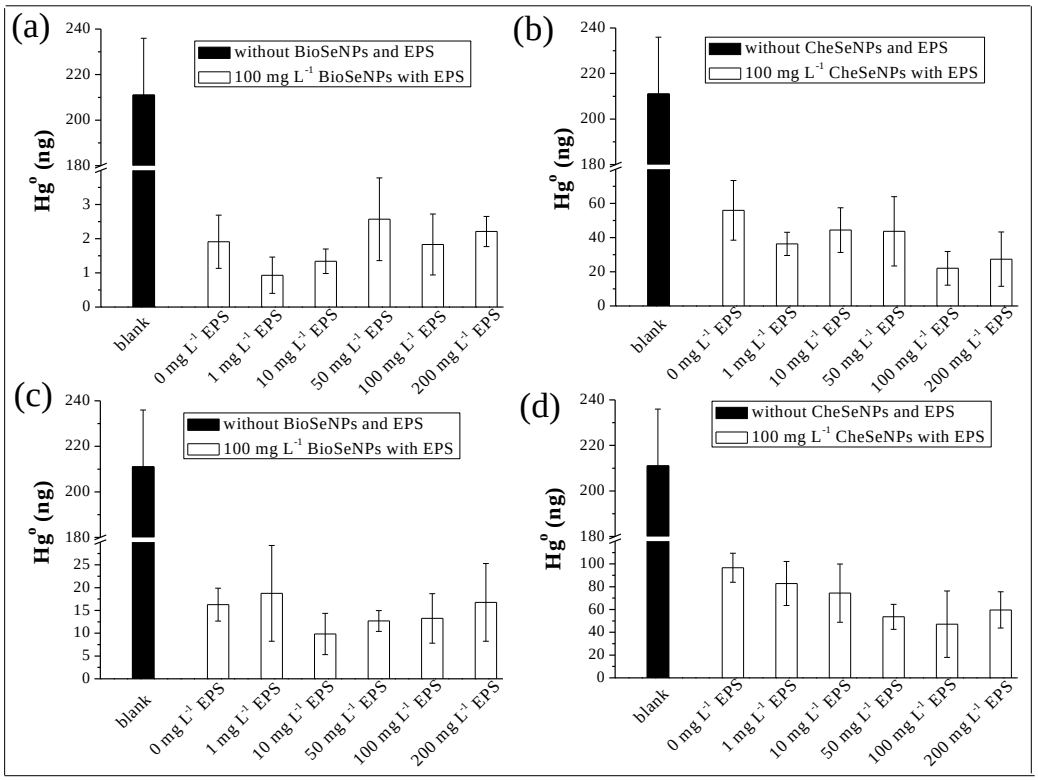


Fig. 7. The effect of EPS on $Hg^0$ immobilization from groundwater using (a) BioSeNPs and (b) CheSeNPs; the effects of EPS on $Hg^0$ remediation of the soil solution using (c) BioSeNPs and (d) CheSeNPs. The blank is the $Hg^0$ contaminated

387 groundwater or soil solution without addition of SeNPs and EPS. Error bars (n=3)
388 represent the standard deviation.

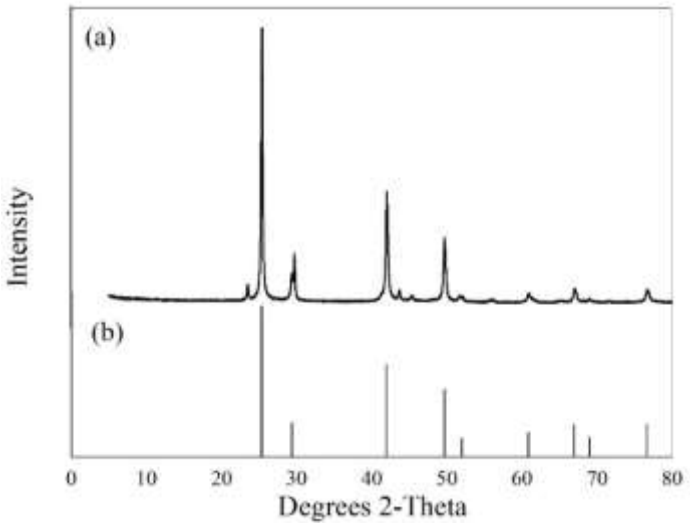


389

390 Fig. 8. XRD pattern of the precipitate collected from CheSeNPs treated $Hg^0$
391 containing ground water. A typical pattern is shown from one of several
392 determinations.

393 Table 1. Total amount of Hg removed from groundwater or soil solution, the amount
394 of Hg in the precipitate, and the proportions of precipitated Hg among the total Hg
395 removed from groundwater or soil solution. All the data are the averages of three
396 replicated measurements. The data are presented as average ± standard deviation.

| | Treatment | Total Hg removed from groundwater (ng) | Hg in the precipitate (ng) | Proportion of precipitated Hg (%) |
|---|---|---|---|---|
| Groundwater | BioSeNPs + 0 mg $L^{-1}$ EPS | 209.1 ± 36.4 | 198.5 ± 2.8 | 94.9 |

| | | | | |
|---|---|---|---|---|
| | BioSeNPs + 1 mg $L^{-1}$ EPS | 210.1 ± 36.0 | 204.3 ± 7.4 | 97.3% |
| | BioSeNPs + 10 mg $L^{-1}$ EPS | 209.7 ± 35.8 | 207.5 ± 13.4 | 98.9% |
| | BioSeNPs + 50 mg $L^{-1}$ EPS | 208.4 ± 36.9 | 194.6 ± 10.2 | 93.4% |
| | BioSeNPs + 100 mg $L^{-1}$ EPS | 209.2 ± 36.5 | 188.2 ± 16.2 | 89.9% |
| | BioSeNPs + 200 mg $L^{-1}$ EPS | 208.8 ± 35.8 | 211.7 ± 6.1 | 101.4% |
| | CheSeNPs + 0 mg $L^{-1}$ EPS | 155.1 ± 59.9 | 142.7 ± 8.1 | 92.0% |
| | CheSeNPs + 1 mg $L^{-1}$ EPS | 174.7 ± 44.9 | 176.39 ± 10.4 | 100.9% |
| | CheSeNPs + 10 mg $L^{-1}$ EPS | 166.6 ± 53.7 | 160.2 ± 19.2 | 96.1% |
| | CheSeNPs + 50 mg $L^{-1}$ EPS | 167.3 ± 63.9 | 180.5 ± 23.6 | 107.9% |
| | CheSeNPs + 100 mg $L^{-1}$ EPS | 188.9 ± 49.2 | 203.6 ± 12.6 | 107.7% |
| | CheSeNPs + 200 mg $L^{-1}$ EPS | 183.6 ± 57.8 | 190.7 ± 3.5 | 103.8% |
| Soil solution | BioSeNPs + 0 mg $L^{-1}$ EPS | 194.7 ± 40.4 | 172.9 ± 13.1 | 88.8% |
| | BioSeNPs + 1 mg $L^{-1}$ EPS | 192.3 ± 50.1 | 200.1 ± 10.4 | 104.1% |
| | BioSeNPs + 10 mg $L^{-1}$ EPS | 201.2 ± 41.7 | 187.8 ± 23.6 | 93.3% |
| | BioSeNPs + 50 mg $L^{-1}$ EPS | 198.3 ± 38.5 | 174.3 ± 11.9 | 87.9% |
| | BioSeNPs + 100 mg $L^{-1}$ EPS | 197.8 ± 42.9 | 190.2 ± 19.3 | 96.2% |
| | BioSeNPs + 200 mg $L^{-1}$ EPS | 194.2 ± 47.3 | 206.4 ± 20.5 | 106.3% |
| | CheSeNPs + 0 mg $L^{-1}$ EPS | 114.4 ± 53.2 | 123.8 ± 22.4 | 108.2% |
| | CheSeNPs + 1 mg $L^{-1}$ EPS | 128.2 ± 62.5 | 140.6 ± 17.5 | 109.7% |

| | | | | |
|---|---|---|---|---|
| | CheSeNPs + 10 mg $L^{-1}$ EPS | 136.6 ± 71.3 | 130.7 ± 27.1 | 95.7% |
| | CheSeNPs + 50 mg $L^{-1}$ EPS | 157.4 ± 50.7 | 170.8 ± 33.5 | 108.5% |
| | CheSeNPs + 100 mg $L^{-1}$ EPS | 163.9 ± 76.5 | 158.2 ± 25.3 | 96.5% |
| | CheSeNPs + 200 mg $L^{-1}$ EPS | 151.4 ± 57.8 | 140.9 ± 33.7 | 93.1% |

## Discussion

This study shows that there was a strong interaction between the SeNPs and the EPS from a selenite-reducing bacterium and this strong binding of EPS to NPs improved the stability of NPs. Nanoparticles tend to bind with EPS.[41] The fluorescence quenching titration data (Fig. 1) confirmed that the fluorescent components, including the tyrosine-like (peak A), the tryptophan-like substances (peak B), the protein-like substances (aromatic I proteins) (peak C) and the protein-like substances (aromatic II proteins) (peak D) have a strong binding ability to the SeNPs.[42,43] The quenching constant ($K_q$, $\times 10^{11}$ L $mol^{-1}$ $sec^{-1}$) (1.59-3.49) for EPS and CheSeNPs was one order of magnitude bigger than the maximum diffusion collision quenching rate constant ($2.0\times10^{10}$ mol $^{-1}$ $sec^{-1}$), implying that the fluorescence quenching process was mainly governed by static quenching which is usually induced by complexation between the fluorophore and the quencher molecules. The binding constant ($K_b$, $\times 10^3$ L $mol^{-1}$) for the complexation of EPS with CheSeNPs ,calculated according to the Hill equation, was found to range from 0.95

414 to 15.9, which is close to the values reported for the binding of toxic metals to EPS.[44]
415 It can be concluded that the binding ability between EPS and CheSeNPs was similar
416 to those between EPS and toxic metals. The binding site number (*n*) for the EPS-
417 CheSeNPs complexes was close to 1 (0.91-1.33), which indicated that there was only
418 one independent class of binding site present in the EPS that participated in trapping
419 CheSeNPs. It can be concluded that the binding of CheSeNPs to EPS was mainly
420 governed by the proteins in the EPS. The FTIR spectra revealed that proteins,
421 carboxylates, polysaccharides and lipids were adsorbed onto CheSeNPs (Fig. 2). The
422 acid-base potentiometric titration curves (Fig. 3) further confirmed binding of
423 proteins, carboxyl and amine groups onto CheSeNPs.[45,46] Adsorption of these
424 functional groups increased the buffering capacity of EPS-capped CheSeNPs.

425 In order to examine the stabilizing effect of EPS on SeNPs, CheSeNPs were
426 used instead of BioSeNPs, because the surface of BioSeNPs are already covered
427 with EPS.[27,47] The zeta potential, hydrodynamic diameter and attachment efficiency
428 data show that EPS from the selenite-reducing bacterium acted as an excellent
429 natural dispersant that can stabilize SeNPs in soil solution or groundwater by
430 inhibition of aggregation (Fig. 4, 5, 6). EPS in the soil solution and groundwater
431 have zeta potential values of about -21 mv and -28 mv, respectively. Adsorption of
432 more negative EPS molecules significantly made SeNPs more negatively charged
433 (Fig. 5). EPS can provide colloidal stability to nanoparticles either by electrostatic,

steric or electrosteric mechanisms.[48,49] In the present study, EPS-capped CheSeNPs were more negatively charged compared to CheSeNPs and this increased the electrostatic force of repulsion between particles and increased the stability of SeNPs.[50] EPS therefore plays an important role in controlling the surface charge of BioSeNPs which will govern the fate of selenium nanoparticles.[22,27] A similar role of EPS on the stability of silver nanoparticles has been documented.[50] However, the effects of EPS on stability of nanoparticles reported in the literature are contradictory. It was found that EPS destabilizes Ag nanoparticles and promotes their aggregation to protect cells.[51] Polysaccharides can also destabilize colloidal particles.[45] The contradictory stabilizing or destabilizing effects of EPS may be relevant to different composition of EPS from different sources. More work is needed to understand the key components that affect the stability of NPs.

Addition of EPS increases stability of SeNPs, associated with the decrease in hydrodynamic diameter, and decreased their settling efficiency (Fig. 6). The stabilizing effect of EPS therefore improves remediation of $Hg^0$ contaminated soil solution and groundwater by CheSeNPs (Fig. 7). For the BioSeNPs treatment group, it was found that when the EPS dosage increased from 1 to 200 mg $L^{-1}$, the remediation efficiency was not significantly increased. Although EPS improves the remediation performance, BioSeNPs were more efficient for $Hg^0$ removal than CheSeNPs. This may be explained because BioSeNPs are covered by EPS during

their synthesis.[52] The EPS bound to the surface of BioSeNPs is helpful for the stability of SeNPs compared with CheSeNPs, and agglomeration of CheSeNPs significantly inhibited the efficiency of mercury remediation. Similarly, 1 mg $L^{-1}$ EPS significantly enhanced remediation performance by BioSeNPs but a higher dosage of EPS inhibited $Hg^0$ removal by BioSeNPs  It is likely that too much EPS blocked $Hg^0$ access to the SeNPs surfaces or chemically passivated the surface through Se-thiol reactions. The immobilization of $Hg^0$ using SeNPs occurs by adsorption or a gas-solid reaction where performance highly depends on surface area. $Hg^0$ capture using bovine serum albumin (BSA) stabilized SeNPs was hindered in comparison with SeNPs synthesized without BSA, despite a huge increase in the available surface area. This was attributed to surface passivation by BSA which decreased the density of available reactive sites on the surface of SeNPs.[52] Similarly, the bacterially derived organic substances bound to the surface of SeNPs increased the stability of SeNPs but too much organic substances may passivate the surface and thus reduce $Hg^0$ removal efficiency.[53,54] These studies are in good agreement with our present study. Generally, a low dosage of EPS (e.g., 1 mg $L^{-1}$) is most cost-effective for enhancing remediation of $Hg^0$ contaminated soil and water by Bio/CheSeNPs from the perspective of an engineering application.

## Conclusions

*C. freundii* Y9 EPS can significantly reduce aggregation and improve the

stability of SeNPs in soil solution and groundwater because of adsorption to SeNPs forming more negatively charged SeNPs. EPS can enhance the remediation efficiency of soil solution and groundwater contaminated with $Hg^0$ using SeNPs. A lower dosage of EPS is most cost-effective for $Hg^0$ remediation of groundwater and a higher dosage is required for remediation of soil solution. This study highlights that the EPS of *C. freundii* Y9 is an excellent natural dispersant of SeNPs and can be used as effective amendment for improving mercury immobilization by SeNPs.

## Acknowledgments

This work was supported by the National Natural Science Foundation of China (U1503281 and U1403181). G. M. Gadd also gratefully acknowledges an award (NE/M01090/1) under the National Environmental Research Council (UK) Security of Supply of Mineral Resources Grant Program: Tellurium and Selenium Cycling and Supply (TeASe).

## Conflict of Interest Disclosure

The authors declare no competing financial interest.

## References

**1.** J. Lahann, *Nat. Nanotechnol.,* 2008, **3**, 320-321.

2. Y. Sun, X. Li, W. Zhang and H.Wang, *Colloids Surf. A Physicochem. Eng. Asp*., 2007, **308**, 60-66.

3. B. Schrick, B. W. Hydutsky, J. L. Blough and T. E. Mallouk, *Chem. Mater.,* 2004, **16**, 2187-2193.
4. F. He, and D. Zhao, *Environ. Sci. Technol.,* 2005, **39**, 3314-3320.
5. R. Kretzschmar, and H. Sticher, *Environ. Sci. Technol.,* 1997, **31**, 3497-3504.
6. J. W. Moreau, R. I. Webb, and J. F. Banfield, *Am. Mineral.,* 2004, **89**, 950-960.
7. J. Dobias, E. I. Suvorova, and R. Bernier-Latmani, *Nanotechnology,* 2011, **22**, 195605.
8. B. Frølund, R. Palmgren, K. Keiding, and P. H. Nielsen, *Water Res.,* 1996, **30**, 1749-1758.
9. J. W. Moreau, P. K. Weber, M. C. Martin, B. Gilbert, I. D. Hutcheon, and J. F. Banfield, *Science,* 2007, **316**, 1600-1603.
10. C. Zhou, Z. Wang, A. Marcus and B. E. Rittmann, *Environ. Sci.: Nano*, 2016, **3**, 1396-1404.
11. S. L. Hockin, and G. M. Gadd, *Appl. Environ. Microbiol.,* 2003, **69**, 7063-7072.
12. S. Hockin, and G. M. Gadd, *Environ. Microbiol.,* 2006, **8**, 816-826.
13. X. Xia, L. Ling and W. Zhang, *Environ. Sci.: Nano*, 2016, **4**, 52-59.
14. N. Ralston, *Nat. Nanotechnol.,* 2008, **3**, 527-528.
15. J. Fellowes, R. Pattrick, D. Green, A. Dent, J. Lloyd, and C. Pearce, *J. Hazard. Mater.,* 2011, **189**, 660-669.
16. X. Wang, D. Zhang, X. Pan, D. J. Lee, F. A. Al-Misned, M. G. Mortuza, and G.

514 M. Gadd, *Chemosphere,* 2017, **170**, 266-273.
515 17.D. Kocman, M. Horvat, and J. Kotnik, *J. Environ. Monit.,* 2004, **6**, 696-703.
516 18.A. García-Sanchez, F. Contreras, M. Adams, and F.Santos, *Environ. Geochem.*
517 *Health,* 2006, **28**, 529-540.
518 19.C. M. Neculita, G. J. Zagury, and L. Deschenes, *J. Environ. Qual.,* 2005, **34**, 255-
519 262.
520 20.K. R. Rolfhus, and W. F. Fitzgerald, *Geochim. Cosmochim. Acta,* 2001, **65**, 407-
521 418.
522 21.Y. Zhang, Z. A. Zahir, and W. T. Frankenberger, *J. Environ. Qual.,* 2004, **33**, 559-
523 564.
524 22.B. Buchs, M. W. Evangelou, L. H. Winkel, and M. Lenz, *Environ. Sci. Technol.,*
525 2013, **47**, 2401-2407.
526 23.S. S. Adav, and D. J. Lee, *J. Hazard. Mater.,* 2008, **154**, 1120-1126.
527 24.M. Dubois, K. A. Gilles, J. K. Hamilton, P. Rebers, and F. Smith, *Anal.*
528 *Chem.,*1956, **28**, 350-356.
529 25.M. M. Bradford, *Anal. Biochem.,* 1976, **72**, 248-254.
530 26.R. Lambert, C. Grant, and S. Sauvé, *Sci. Total Environ.,* 2007, **378**, 293-305.
531 27.R. Jain, N. Jordan, S. Weiss, H. Foerstendorf, K. Heim, R. Kacker, R. Hübner, H.
532 Kramer, E. D. van Hullebusch, F. Farges, and P. N. L. Lens, *Environ. Sci. Technol.,*
533 2015, **49**, 1713-1720.

28. Y. Cui, L. Li, N. Zhou, J. Liu, Q. Huang, H. Wang, J. Tian, and H. Yu, *Enzyme Microb. Technol.,* 2016, **95**, 185-191.
29. K. Gai, T. P. Hoelen, H. Hsu-Kim, and G. V. Lowry, *Environ. Sci. Technol.,* 2016, **50**, 3342-3351.
30. M. R. Eftink, in *Topics in Fluorescence Spectroscopy,* eds. J. R. Lakowicz, Springer, German, 2002, pp. 53-126.
31. T. L. Hill,. *Cooperativity Theory in Biochemistry: Steady-state and Equilibrium Systems*, Springer Science & Business Media, 2013.
32. L. Zhu, H. Qi, Y. Kong, Y. Yu, and X. Xu, *Bioresour. Technol.,* 2012, **124**, 455-459.
33. J. Schmitt, and H. C. Flemming, *Int. Biodeterior. Biodegradation,* 1998, **41**, 1-11.
34. X. Wei, L. Fang, P. Cai, Q. Huang, H. Chen, W. Liang, and X. Rong, *Environ. Pollut.,*2011, **159**, 1369-1374.
35. X. Sun, S. Wang, X. Zhang, J. Chen, X. Li, B. Gao, and Y. Ma, *J. Colloid Interface Sci.,* 2009, **335**, 11-17.
36. K. Kavita, A. Mishra, and B. Jha, *Biofouling,* 2011, **27**, 309-317.
37. Z. Liang, W. Li, S. Yang, and P. Du, *Chemosphere,* 2010, **81**, 626-632.
38. P. V. Bramhachari, P. B. K. Kishor, R. Ramadevi, R. Kumar, B. R. Rao, and S. K. Dubey, *J. Microbiol. Biotechnol.,* 2007, **17**, 44-51.
39. K. Kavita, V. K. Singh, A. Mishra, B. Jha, *Carbohydr. Polym.,* 2014, **101**, 29-35.

554 40. B. Lartiges, S. Deneux-Mustin, G. Villemin, C. Mustin, O. Barres, M. Chamerois,
555 B. Gerard, and M. Babut, *Water Res.,* 2001, **35**, 808-816.
556 41. W. D. Burgos, J. T. McDonough, J. M. Senko, G. Zhang, A. C. Dohnalkova, S.
557 D. Kelly, Y. Gorby, and K. M. Kemner, *Geochim. Cosmochim. Acta,* 2008, **72**,
558 4901-4915.
559 42. X. Pan, J. Liu, and D. Zhang, *Colloids Surf. B Biointerfaces,* 2010, **80**, 103-106.
560 43. W. Song, X. Pan, S. Mu, D. Zhang, X. Yang, and D. J. Lee, *Bioresour. Technol.,*
561 2014, **160**, 119-122.
562 44. G. Guibaud, E. van Hullebusch, and F. Bordas, *Chemosphere,* 2006, **64**, 1955-
563 1962.
564 45. J. Buffle, K. J. Wilkinson, S. Stoll, M. Filella, and J. Zhang, *Environ. Sci.*
565 *Technol.,*1998, **32**, 2887-2899.
566 46. U. Gupta, H. B. Agashe, N. K. Jain, *J. Pharm Pharm. Sci.,* 2007, **10**, 358-367.
567 47. R. Jain, N. Jordan, S. Tsushima, R. Hübner, S. Weiss and P. Lens, *Environ. Sci.:*
568 *Nano*, 2017, **4**, 1054-1063.
569 48. A. M. E. Badawy, T. P. Luxton, R. G. Silva, K. G. Scheckel, M. T. Suidan, and T.
570 M. Tolaymat, *Environ. Sci. Technol.,* 2010, **44**, 1260-1266.
571 49. K. Ikuma, A. S. Madden, A. W. Decho and B. L. Lau, *Environ. Sci.: Nano*, 2014,
572 **1**, 117-122.
573 50. S. S. Khan, A. Mukherjee, and N. Chandrasekaran, *Water Res.,* 2011, **45**, 5184-

574 5190.
575 51.N. Joshi, B. T. Ngwenya, and C. E. French, *J. Hazard. Mater.,* 2012, **241**, 363-
576 370.
577 52.N. C. Johnson, S. Manchester, L. Sarin, Y. Gao, I. Kulaots, and R. H. Hurt,
578 *Environ. Sci. Technol.,* 2008, **42**, 5772-5778.
579 53.N. T. Prakash, N. Sharma, R. Prakash, K. K. Raina, J. Fellowes, C. I. Pearce, J.
580 R. Lloyd, and R. A. D. Pattrick, *Biotechnol. Lett*. 2009, **31**, 1857-1862.
581 54.C. Pearce, R. A. D. Pattrick, N. Law, J. M. Charnock, V. S. Coker, J. W. Fellowes,
582 R. S. Oremland, and J. R. Lloyd, *Environ. Technol*. 2009, **30**, 1313–1326.